Electronic Supplementary Information (ESI)

Stimuli-responsive noniridescent structural color of thin-film coating based on multilayered nanosheets preserving interlayer space

Yuka Kitamura,[1] Hisafumi Sudo,[1] Hiroaki Imai,[1] Yui Maejima,[2] Michinari Kohri,[2] Yuya Oaki*[1],

[1] Department of Applied Chemistry, Faculty of Science and Technology, Keio University, 3-14-1 Hiyoshi, Kohoku-ku, Yokohama 223-8522, Japan

[2] Department of Applied Chemistry and Biotechnology, Graduate School of Engineering, Chiba University, 1-33 Yayoi-cho, Inage-ku, Chiba 263-8522, Japan

E-mail: oakiyuya@applc.keio.ac.jp

Contents

Experimental methods

Preparation of the nanosheets. The precursor layered materials were synthesized by the intercalation of the guest molecules in the layered niobate (Table 1). The synthetic procedure was described in our previous reports.[52,53] The resultant layered composites (60 mg) were dispersed in 24 cm^3 of purified water or ethanol (Fuji-Wako, 99.5 %) in a glass vial (50 cm^3 in volume) and then sonicated using an ultrasonic homogenizer (Branson, 250 W, output 50 %). The probe was set 1 cm below the liquid interface. The sonication was performed for 30 min in a water bath. The temperature was kept below room temperature in water bath. After the unexfoliated and bulk objects were filtered using a commercial cotton, 5–150 mm^3 (V_{ns}) of the resultant dispersion liquid containing the surface modified nanosheets were dropped on a piece of cleaned silicon (Si) substrate heated at T_s = 100–180 °C using a temperature-controlled stage. A commercial polished Si substrate was rinsed with immersion in the mixture of 11.3 mol dm^{-3} HCl aqueous solution and methanol (1/1 by volume) and sulfuric acid for 1 h. Then, the substrate was rinsed with purified water and acetone.

Structural characterization. The morphologies of the nanosheets were observed by transmission electron microscopy (TEM, FEI Tecnai G2) operated 120 or 200 kV and atomic force microscopy (AFM, Shimadzu SPM-9700HT). Optical microscopy (Keyence VHX-970F), laser microscopy (Keyence VK-X1000), and scanning electron microscopy (SEM, FEI Inspect F50) were used to observe the thin-film coatings. The layered crystal structures of the precursor and nanosheet coating were analyzed by X-ray diffraction (XRD, Bruker D8-Advance) with Cu-Kα radiation. UV-Vis spectra were measured by a spectrophotometer using an integrated sphere (JASCO, V-670). The diffuse reflectance spectra were measured for the coatings on Si substrate after the background was collected using solid powder of magnesium oxide. UV-Vis spectra with changing ($\theta_i = \theta_r$) was carried out using another spectrophotometer (JASCO V-650/ARSV-732).

Sensing of biogenic amines. The following amines were purchased and used without further purification: histamine dihydrochloride (Hst, TCI 98.0 %), 1,4-diaminobutane (Put, TCI 98.0 %), 2-phenylethylamine (Phm, TCI 98.0 %), tyramine (Tym, TCI 98.0 %), 1,5-diaminopentane (Cad, TCI 98.0 %), and 4-aminobutyric acid (Aba, TCI 99.0 %). Aqueous solutions of these amines and their mixtures were prepared with purified water in the concentration range of 10^{-5} and 10^{-2} mol dm^{-3}. The thin film exhibiting the structural color was heated at 60 °C. The initial x value of the nanosheet thin film was estimated from the photograph of optical microscopy (Keyence VHX-970F) under the magnification of ×50. After taking the photograph at the initial state, 20 mm^3 of the amine solution was dropped on the film. The movie was taken for 6 min after dropping the solution. The photograph was taken 5 min after

the evaporation of water. The Δx value was calculated using RGB values on the trimmed optical microscopy image 0.5 × 0.5 mm by the following (Eqs. S1 and S2).

$$\begin{bmatrix} X \\ Y \\ Z \end{bmatrix} = \begin{bmatrix} 0.4124 & 0.3576 & 0.1805 \\ 0.2126 & 0.7152 & 0.0722 \\ 0.0193 & 0.1192 & 0.9505 \end{bmatrix} \begin{bmatrix} R \\ G \\ B \end{bmatrix} \quad \ldots \text{(Eq. S1)}$$

$$(x, y) = \left(\frac{X}{X+Y+Z}, \frac{Y}{X+Y+Z} \right) \ldots \text{(Eq. S2)}$$

The XRD patterns of the films were measured before and after the exposure to the amine solutions.

Previous reports about sensing biogenic amines

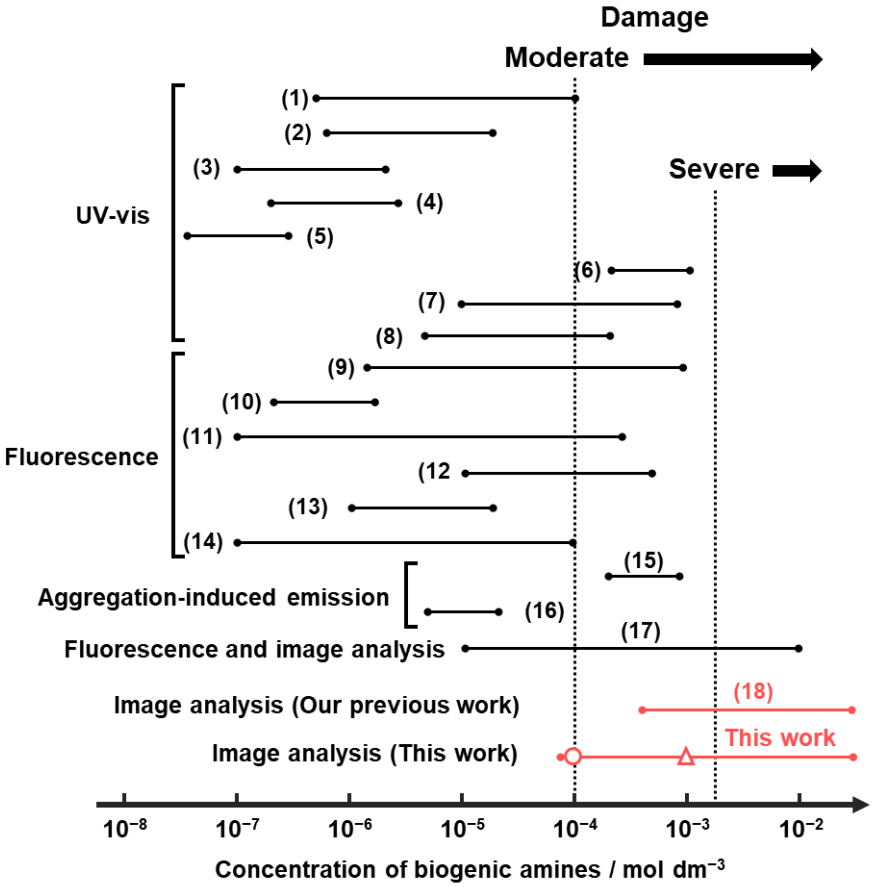

Fig. S1. Detection rages of biogenic amines in previous reports. The diagram in our previous was modified.[48]

The lower limit of the detection was improved for Hst, Put, Tym, and Phm (circle in Fig. S1) compared with that in our previous work (18).[48] In addition, our present device has no selectivity to these biogenic amines. As the total amount of the amine mixtures caused the health damage, the nonselective detection is important.

Additional References

(1) T. Sato, T. Horiuchi and I. Nishimura, *Anal. Biochem*., 2005, **346**, 320.

(2) K. M. A. El−Nour, E. T. A. Salam, H. M. Soliman and A. S. Orabi, *Nanoscale Res. Lett.*, 2017, **12**, 231.

(3) C. Huang, S. Wang, W. Zhao, C. Zong, A. Liang, Q. Zhang and X. Liu, *Microchim. Acta*, 2017, **184**, 2249.

(4) S. Chopra, A. Singh, P. Venugopalan, N. Singh and N. Kaur, *ACS Sustain. Chem. Eng*.,

2017, **5**, 1287.
(5) S. Teepoo, A. Promta and P. Phapugrangkul, *Food Anal. Methods*, 2019, **12**, 1886.
(6) R. Lv, X. Huang, C. Dai, W. Ye and X. Tian, *J. Food Process Eng.*, 2019, **42**, e13099.
(7) A. Orouji, F. Ghasemi, A. Bigdeli, M. R. Hormozi-Nezhad, *ACS Appl. Mater. Interfaces*, 2021, **13**, 20865.
(8) Y. Fukushima and S. Aikawa, *Tetrahedron Lett.*, 2021, **72**, 153088.
(9) H. A. Azab, S. A. El−Korashy, Z. M. Anwar, G. M. Khairy, M. S. Steiner and A. Duerkop, *Analyst*, 2011, **136**, 4492.
(10) S. Chopra, J. Singh, H. Kaur, A. Singh, N. Singh and N. Kaur, *Eur. J. Inorg. Chem.*, 2015, **26**, 4437.
(11) X. Y. Xu, X. Lian, J. N. Hao, C. Zhang and B. Yan, *Adv. Mater*., 2017, **29**, 1605739.
(12) A. I. Danchuk, N. S. Komova, S. N. Mobarez, S. Y. Doronin, N. A. Burmistrova, A. V. Markin and A. Duerkop, *Anal. Bioanal. Chem*., 2020, **412**, 4023.
(13) G. Munzi, S. Failla and S. Di Bella, *Analyst*, 2021, **146**, 2144.
(14) Z. Wang, F. Liu and C. Lu, *Biosens. Bioelectron*., 2014, **60**, 237.
(15) M. Nakamura, T. Sanji and M. Tanaka*, Chem.− A Eur. J*., 2011, **17**, 5344.
(16) T. Kim and Y. Kim, *Chem. Commun*., 2016, **52**, 10648.
(17) M. S. Steiner, R. J. Meier, A. Duerkop and O. S. Wolfbeis, *Anal. Chem*., 2010, **82**, 8402.
(18) Ref 48 in the main text.

Lateral size and thickness of the nanosheets

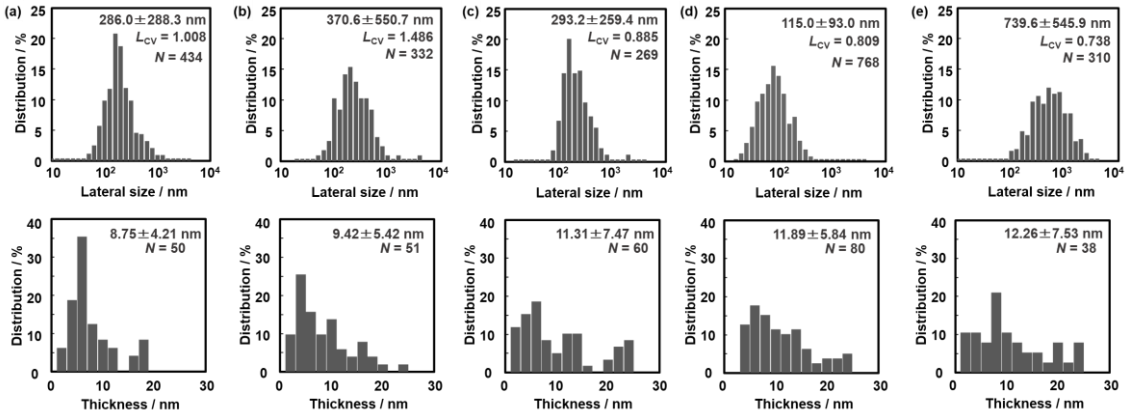

Fig. S2. Histograms of the lateral-size (upper panels) and thickness (lower panels) distributions. (a) CN-BA-modified niobate nanosheets exfoliated in water. (b) API-modified niobate nanosheets exfoliated in water. (c) DAMN-modified niobate nanosheets exfoliated in water. (d) CN-BA-modified niobate nanosheets exfoliated in ethanol. (e) DEA-modified niobate nanosheets exfoliated in ethanol. The coefficient of the variation (L_{CV}) was calculated by dividing mean by average to compare the polydispersity of the lateral size.

The lateral size and thickness were measured on the TEM and AFM images with the number of samples (n) noted in the panels, respectively.

Relationship between the coating conditions and colors

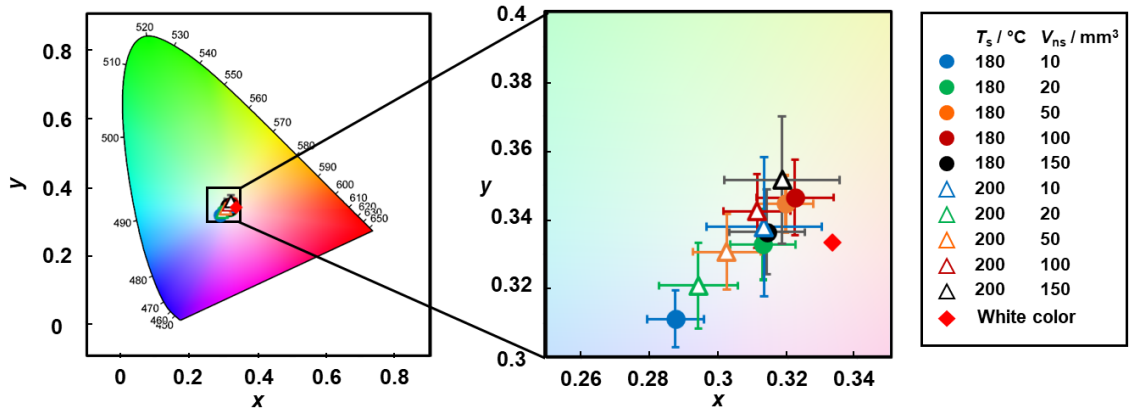

Fig. S3. Chromaticity of the thin films based on the CN-BA-niobate nanosheets prepared under the different coating conditions.

The brightest blue color was obtained at C_{ns} = 2.5 g dm^{-3}, T_s = 180 °C, and V_{ns} = 10 mm^3 (filled blue plot in Fig. S3). The coating conditions were optimized by changing T_s and V_{ns} after the concentration was fixed to C_{ns} = 2.5 g dm^{-3} (the range (i) in Fig. 3a). The coating condition with the shortest distance to the white color was suitable to achieve the brightest color.

References of the thin films

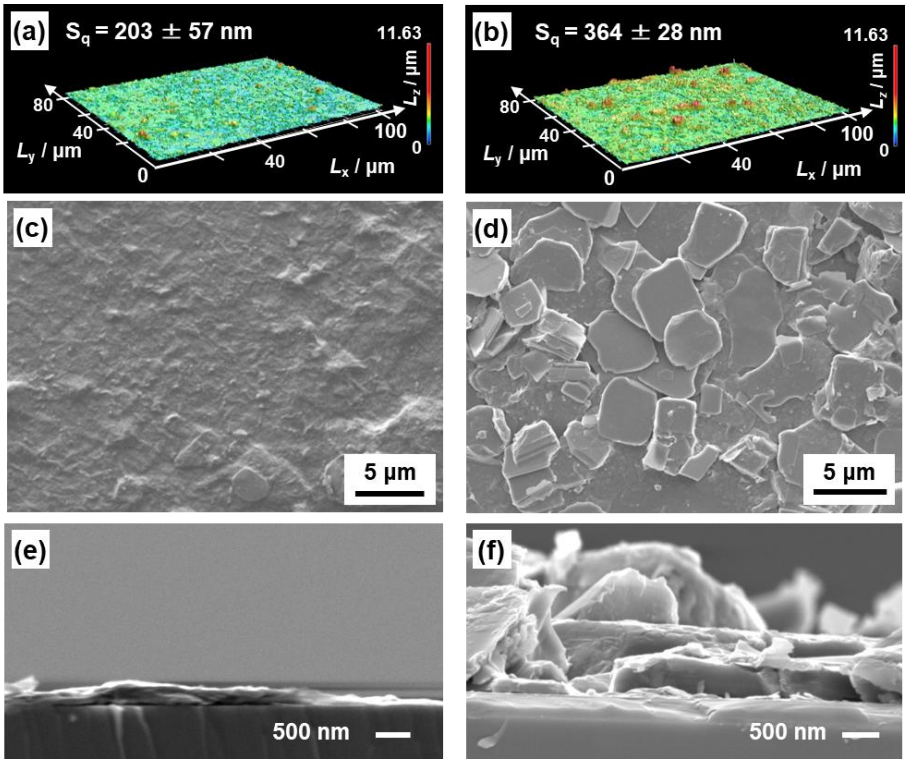

Fig. S4. Laser microscopy (a,b) and surface (c,d) and cross-sectional SEM (c–f) images of the nanosheet thin films. (a,c,e) Sample A: the thin film exhibiting the structural color at the initial coating conditions C_{ns} = 2.5 g dm^{-3}, T_s = 140 °C, and V_{ns} = 50 mm^3 before the optimization of the coating conditions. (b,d,f) Thin film without the structural color at C_{ns} = 2.5 g dm^{-3}, T_s = 100 °C, and V_{ns} = 50 mm^3.

Additional data for sensing of biogenic amines

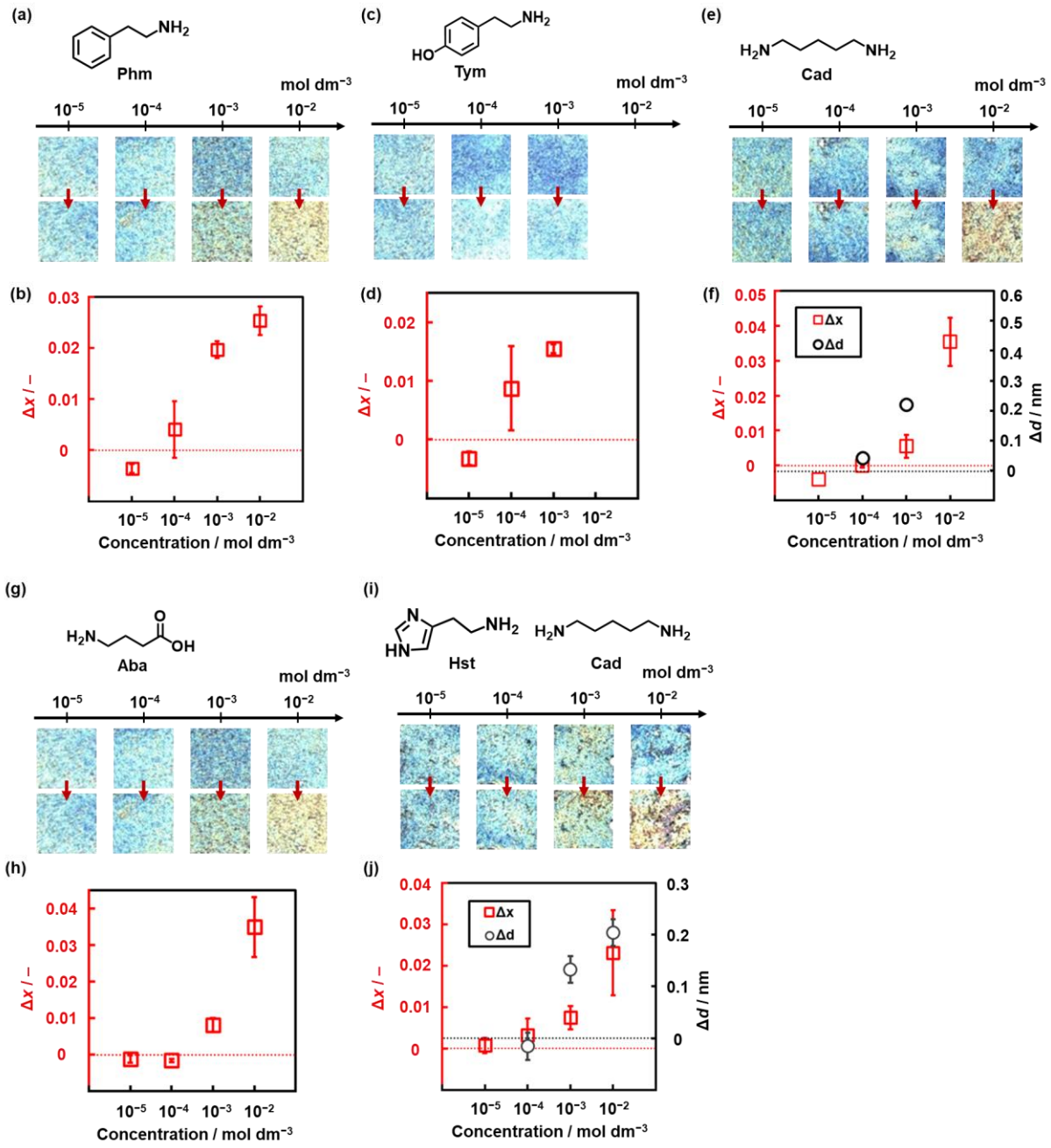

Fig. S5. Colorimetric detection of the other biogenic amine Phm (a,b), Tym (c,d), Cad (e,f), Aba (g,h), and mixture of Hst and Cad (i,j). (a,c,e,g,i) Molecular structures and changes in the optical microscopy images before and after dropping the aqueous solutions containing the amines. (b,d,f,g,i) Relationship between the amine concentration, Δx calculated from the optical microscopy images (left axis), and Δd_0 measured from the XRD patterns (right axis).

XRD patterns of the amine intercalation for sensing

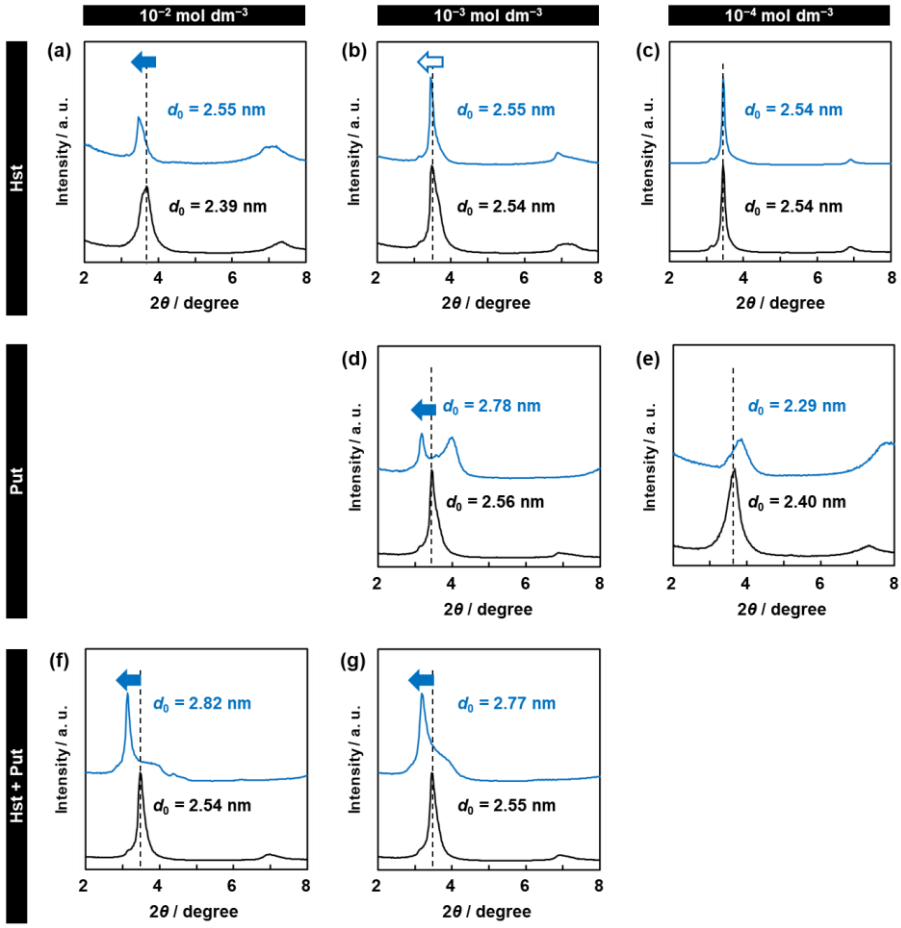

Fig. S6. XRD patterns of the thin film coatings before (black) and after (blue) the exposure to the biogenic amines, namely Hst (a–c), Put (d,e), and the mixture of Hst and Put (f,g) at 10^{-2} (a,f), 10^{-3} (b,d,g), and 10^{-4} (c,e) mol dm^{-3}.

In the XRD patterns (Fig. S6), the samples with the blue arrows showed the significant changes in Δx and Δd_0 in Fig. 5, whereas the changes in Δx were only observed for the sample with the white arrow. The peak shift corresponds to the expansion of the interlayer space depending on the amount of the intercalated amines.

XRD patterns of the Hst- and Cad-intercalated layered niobate

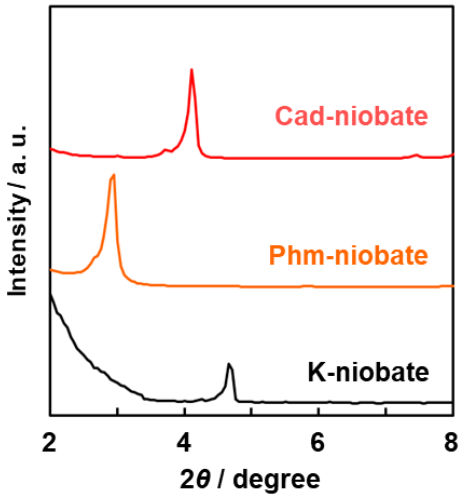

Fig. S7. XRD patterns of the pristine potassium-ion, Phm-, and Cad-intercalated niobates,

These guest-intercalated niobates were synthesized by the same method as that for CN-BA-niobate. In the intercalated states, d_0 was 2.99 nm for Phm and 2.15 nm for Cad.

Reference experiments for sensing

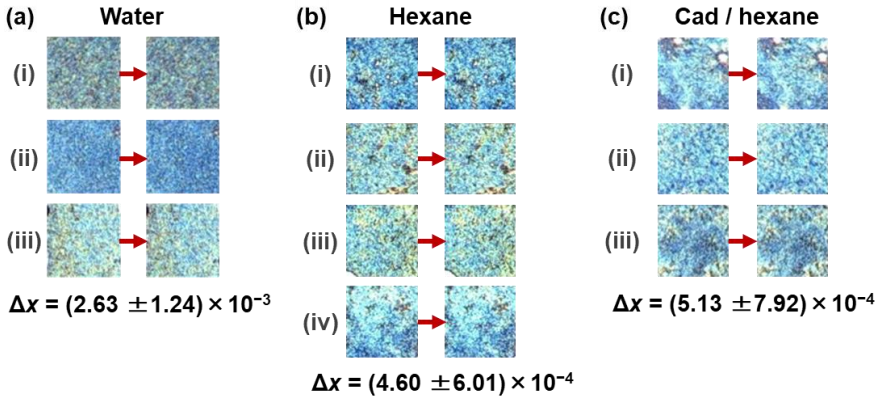

Fig. S8. Optical microscopy images of the thin-film coatings before (left) and after (right) dropping purified water (a), hexane (b), and hexane solution containing Cad (b).

Aqueous solutions containing the biogenic amines was used for the sensing experiments (Fig. 5 and Fig. S5). The reference experiments were performed by dropping only water and hexane (Fig. S8a,b). No visible color changes and distinct changes in the average Δx, namely $(2.63 \pm 1.24) \times 10^{-3}$ for water and $(4.60 \pm 6.01) \times 10^{-4}$ for hexane, were observed.

When the amine (Cad) solution was prepared with hexane instead of water, the color change was not induced by dropping the hexane solution (Fig. S8c). The average Δx was $(5.13 \pm 7.92) \times 10^{-4}$. The results imply that Cad is preferred to be solvated in hexane rather than intercalated in the interlayer space of the CN-BA-modified niobate. Therefore, the affinity of the biogenic amines to water, hexane, and CN-BA is calculated using HSP distance in Table S1.

HSP distance of biogenic amines to solvents

Table S1. HSP distance of biogenic amines to water, hexane, and CN-BA.

	Water (solvent)	Hexane (solvent)	CN-BA (guest)
Histamine (Hst)	31.16	18.32	5.85
Cadaverine (Cad)	34.72	11.57	7.56
Putrescine (Putr)	33.66	12.64	7.59
Tyramine (Tym)	31.71	16.89	7.16
2-Phenylethylamine (Phm)	37.54	10.86	6.38

HSP distance was calculated using HSP in practice as a commercial software (HSP-ip). In all these amines, the HSP distance between amine and interlayer CN-BA was significantly smaller than that between amine and water. The fact implies that these amines are preferentially introduced in the interlayer space from the aqueous solution. In contrast, the HSP distance between amine and interlayer CN-BA was not so significantly smaller than that between amine and hexane. As the HSP distances have no distinct differences, the amines are not introduced into the interlayer space but dissolved in hexane. The calculation supports the experimental results in Fig. S8.